Received: 9 December 2023 | Revised: 4 March 2024 | Accepted: 25 April 2024 | Published online: 30 April 2024

RESEARCH ARTICLE

Journal of Optics and Photonics Research
2024, Vol. 1(3) 131–144
DOI: 10.47852/bonviewJOPR42022261

BON VIEW PUBLISHING

Intrinsic and Extrinsic Scattering and Absorption Coefficients New Equations in Four-flux and Two-flux Models Used for Determining Light Intensity Gradients

David Barrios Puerto[1],*

[1]*Universidad Carlos III de Madrid, Spain*

Abstract: Collimated, diffuse, and total light intensity gradients, for forward and backward light senses, were determined in a three substrate layers – glass/electrolyte/glass – almost transparent sample, using optical constants and new equations for intrinsic and extrinsic scattering and absorption coefficients. These new equations were obtained for the inner electrolyte layer from the systems of differential equations of the four-flux and two-flux radiative transfer models, used for determining intrinsic and extrinsic coefficients, respectively, once knowing the optical constants of outer glass layers, from a single glass substrate sample measured in advance. Extinction coefficients were determined from optical constants and considering the wavelength compression of light when it enters into a material, decreasing its speed with respect to the vacuum. The same extinction coefficients for glass and electrolyte layers were computed in three different ways. First, from optical constants, they were determined using collimated transmittance and reflectance solutions of four-flux model. From them, collimated interface reflectance and attenuation due to extinction were computed. These intermediate parameters for glass and electrolyte layers were required for determining inner collimated light intensities at the interfaces, which were used at the collimated forward and backward differential equations, solving for the forward and backward extinction coefficients. The three-extinction matching requirement was successfully satisfied for the glass and electrolyte layers. Two average crossing parameters equations, for each sense, and four forward scattering ratios equations, for collimated and for diffuse light intensities for each sense, were used in the system of diffuse differential equations (*DDE*) for intrinsic coefficients. For them, intuitive equations were proposed based on collimated and diffuse light intensities at each interface. New equations for extrinsic parameters were determined by equalizing the system of total differential equations of the two-flux model to the sum of the systems of collimated and *DDE* of the four-flux model.

Keywords: scattering and absorption coefficients, average crossing parameter, forward scattering ratio, four-flux model, two-flux model

1. Introduction

The inverse problem of absorption and scattering of light by small particles, from the transmittance (T) and reflectance (R) measurements, was defined in Bohren and Huffman [1] as the hard problem. The direct problem, defined as the easy problem, considers input data such as concentration, shape, size, and refractive index of particles and surrounding medium. When the size of the particles is of the order or bigger than the incident wavelength, scattering of light, besides absorption, becomes important and the Lorenz–Mie theory provides a solution for the single scattering direct problem [2]. Mie explicitly solved Maxwell's electromagnetic equations and investigated the scattering of a single spherical particle in a non-absorbing matrix for a wide range of sizes. Because of the work coming from Lorenz, the complete solution was called the Lorenz-Mie theory that was extensively summarized for small and large particles in [1, 3, 4] and for complex shapes of particles different than spherical [5]. Inhomogeneities in heterogeneous materials are associated with a macroscopic dielectric permeability and the optical properties are governed by a spatial average, which is expressed through an appropriate effective medium theory [6]. If the inhomogeneities in the composite medium are large enough, the effective medium theories are not valid and radiative transfer theories [7, 8] such as the two-flux model (2FM) and four-flux model (4FM) are used instead [9]. Multiple scattering and radiative transfer calculations, of great importance in many areas of science and technology [4, 9], were used to compare four-flux calculations of T in previous works [10, 11]. Two-flux model considers two diffuse light beams in opposite senses, forward (i) and backward (j) [12], at the differential equations relating extrinsic scattering and absorption coefficients, leading to the hyperbolic solution for R. Two collimated light beams were added besides for the 4FM [13]. Scattering and absorption cross sections were related to intrinsic scattering and absorption coefficients of the 4FM in Maheu et al. [14] for the diffuse differential equations (*DDE*), leading to the solutions for collimated-diffuse T (T_{cd}) and R (R_{cd}), that is, the diffuse T and R when illuminating with collimated light. Extinction

*Corresponding author: David Barrios Puerto, Universidad Carlos III de Madrid, Spain. Email: dbarrios@ing.uc3m.es. The research was conducted at Universidad Carlos III de Madrid, Spain. Correspondence concerning this article should be addressed to dbarriosp76@gmail.com

coefficients, that is, the sum of the intrinsic scattering and absorption coefficients, are involved into the collimated differential equations (*CDE*), leading to the solutions for collimated-collimated T (T_{cc}) and R (R_{cc}), that is, the collimated T and R when illuminating with collimated light. Although 2FM was originally designed for completely diffuse samples, it can be approximated for samples showing partly collimated and partly diffuse light transmitted and reflected [15], considering the differential equations of 2FM as total differential equations (TDE). The hyperbolic solution of the 2FM for T was given in Maheu and Gouesbet [16]. A correction was considered for taking into account the interfaces [17], leading to the solutions for total T (T_t) and R (R_t). If 2FM is considered for total instead of diffuse T and R, diffuse fractions of light at the interfaces are required for determining total interface reflectance, computed as the sum of collimated and diffuse components [15].

Collimated interface reflectance (r_c), determined from optical constants (complex refractive index) using Fresnel transmission and reflection coefficients averaged for both light polarizations, shows a bidirectional behavior, that is, obtaining the same value for light traveling from the faster to the slower mediums and vice versa. Despite other works [15, 18, 19] indicating the opposite, diffuse interface reflectance (r_d) also must show a bidirectional behavior when considering the suggestion of Kottler [20] using the critical angle (θ_c) of total internal reflection (TIR) as the limit of integration, instead of 90°, following the expression for computing r_d of [21]. The bidirectionality of r_d was observed in a previous work of Barrios et al. [22], using the optical T and R measurements of a suspended particle device (*SPD*) smart window, at both optical states, that is, dark OFF and clear ON, without and with applied voltage, respectively. Extrinsic scattering and absorption coefficients for the *SPD* sample were determined in Barrios et al. [22], considering total T and R for approximated 2FM method and using the appropriate r_d, solving mistakes of fittings observed in previous works with the same *SPD* sample when no bidirectional r_d had been considered. Intrinsic scattering and absorption coefficients of 4FM for the *SPD* sample were also determined in Barrios et al. [22], thanks to a new proposed fifth equation required for solving the system of four equations (for T_{cc}, R_{cc}, T_{cd}, and R_{cd}) and five unknowns appearing at the solutions of the 4FM [14]. The procedure carried out in Barrios et al. [22] for the *SPD* sample, studied in a single-layer method, was divided into three steps. At the first step, optical constants were determined from collimated regular T (T_{reg}) and specular R (R_{spe}) measurements using 4FM T_{cc} and R_{cc} solutions [14]. Extrinsic scattering and absorption coefficients were determined from total T (T_{tot}) and total R (R_{tot}) measurements using 2FM T_t and R_t solutions in the second step [14–17]. The third step consisted of determining intrinsic scattering and absorption coefficients from diffuse T (T_{dif}) and diffuse R (R_{dif}) measurements using 4FM T_{cd} and R_{cd} solutions [14], being the unknowns the intrinsic scattering coefficients and the forward scattering ratio (FSR). Intrinsic absorption coefficients were determined subtracting intrinsic scattering coefficients to extinction coefficients, being this one computed from optical constants. The new equation proposed in Barrios et al. [22], for the average crossing parameter (*ACP*), was computed from collimated and diffuse light intensities at the interfaces, knowing that $ACP = 1$ when $T_{dif} = R_{dif} = 0$ (i.e., $T_{reg} = T_{tot}$ and $R_{spe} = R_{tot}$) and $ACP = 2$ when $T_{reg} = R_{spe} = 0$ (i.e., $T_{dif} = T_{tot}$ and $R_{dif} = R_{tot}$). A value of $ACP = 3^{0.5}$ was considered for the homogeneous clouds of Venus in Sagan and Pollack [23] (i.e., considering that light travels the same distance in the three axis, i.e., the main diagonal of a cube of side unity). Although the magnitude of the fluxes is irradiance (mW/m^2 per nm), they are considered unitless and normalized to the forward collimated light beam, since the samples are only forward illuminated through the front interface at the optical characterization process. Intrinsic and extrinsic scattering and absorption coefficients are expressed in m^{-1} units. The rest of the parameters, that is, r_c, r_d, and FSR, and also all collimated, diffuse, and total light intensities are unitless, with values varying from 0 to 1. The single-layer method used with the *SPD* [22] sample was tested successfully with a polymer dispersed liquid crystal (*PDLC*) smart window sample, at the translucent OFF and at the transparent ON optical states.

A multilayer collimated study of the *SPD* sample was carried out in Barrios and Alvarez [24], following multilayer matrixial methods [25–28]. The optical constants of the inner active layer of the *SPD* sample were determined using the optical constants of the glass outer substrate layers and indium-doped tin oxide (*ITO*) transparent conductor thin film layers, both determined in advance from two separated samples (i.e., a glass and an *ITO*-glass) and considering five layers at the sandwich structure (i.e., glass/*ITO*/*SPD*/*ITO*/glass). The inner *SPD* active layer, of thickness higher than incident light wavelength of the solar spectrum range, was hence considered also as substrate and not as a thin film. However, the new equation for ACP [22] was not consistent with the multilayer diffuse study of the *SPD*. In order to obtain the intrinsic and extrinsic scattering and absorption coefficients in a multilayer method, the current work describes the 4FM new equations discovered by its author in another recent work [29], using a three-substrate-layer sample, that is, a glass/electrolyte/glass (*GEG*) sample. Besides *SPD* and *PDLC*, electrochromic devices (*ECD*s) are another type of electrically controllable smart window technology. As explained in Barrios Puerto [29], the inner electrolyte (E) substrate layer of the *GEG* sample was also used in a WO_3-NiO inorganic-based *ECD*, using fluorine-doped tin oxide (*FTO*) instead of *ITO*, since indium element is rare in nature. The sandwich structure of the whole *ECD* was glass/*FTO*/WO_3/E/NiO/*FTO*/glass, considering *FTO*, WO_3, and NiO as thin film layers and glass and *E* as substrate layers. The optical appearance of WO_3 and NiO are transparent colorless without applied voltage. With a low DC applied voltage, a redox reaction takes place between cathodic WO_3 and anodic NiO inner active layers, changing the optical appearance to bluish, for WO_3, and to brownish, for NiO, that is, obtaining a neutral gray optical appearance for the whole *ECD* at the colored ON optical state and a transparent colorless optical appearance at the bleached OFF optical state.

In this work, it is detailed the new method discovered in Barrios Puerto [29] for obtaining intrinsic scattering and absorption coefficients, carried out with the three-substrate-layer sample, that is, *GEG* multilayer sample, and using the *CDE* and the *DDE* of the 4FM [13, 14]. Instead of one ACP and one FSR parameters, as in T_{cd} and R_{cd} solutions of reference [14], two ACPs and four FSRs were required in Barrios Puerto [29]. As a novelty in relation to reference [29], the new equations for obtaining extrinsic scattering and absorption coefficients were discovered, using the TDE of the 2FM [12] and knowing that the TDE can be computed as the sum of the collimated and the *DDE*, that is, TDE = *CDE* + *DDE*. The new equations retrieved for all the parameters of the 4FM and of the 2FM (dependent on the parameters of the 4FM) are explained in detail in the present paper. The compression of wavelength of light when it enters into a slower medium (keeping constant its frequency when modifying the speed of light) was considered for obtaining the extinction coefficients from the optical constants retrieved from the first step of the previous method [22], that is, fitting T_{reg} and R_{spe} to T_{cc} and R_{cc} 4FM solutions, respectively [14]. Then, the same spectral value for the extinction coefficients than the obtained from the

Figure 1
Sandwich structure of the glass/electrolyte/glass (*GEG*) sample. (a) Collimated and diffuse light intensities of the four-flux model and (b) Total light intensities of the two-flux model (computed as the sum of collimated and diffuse)

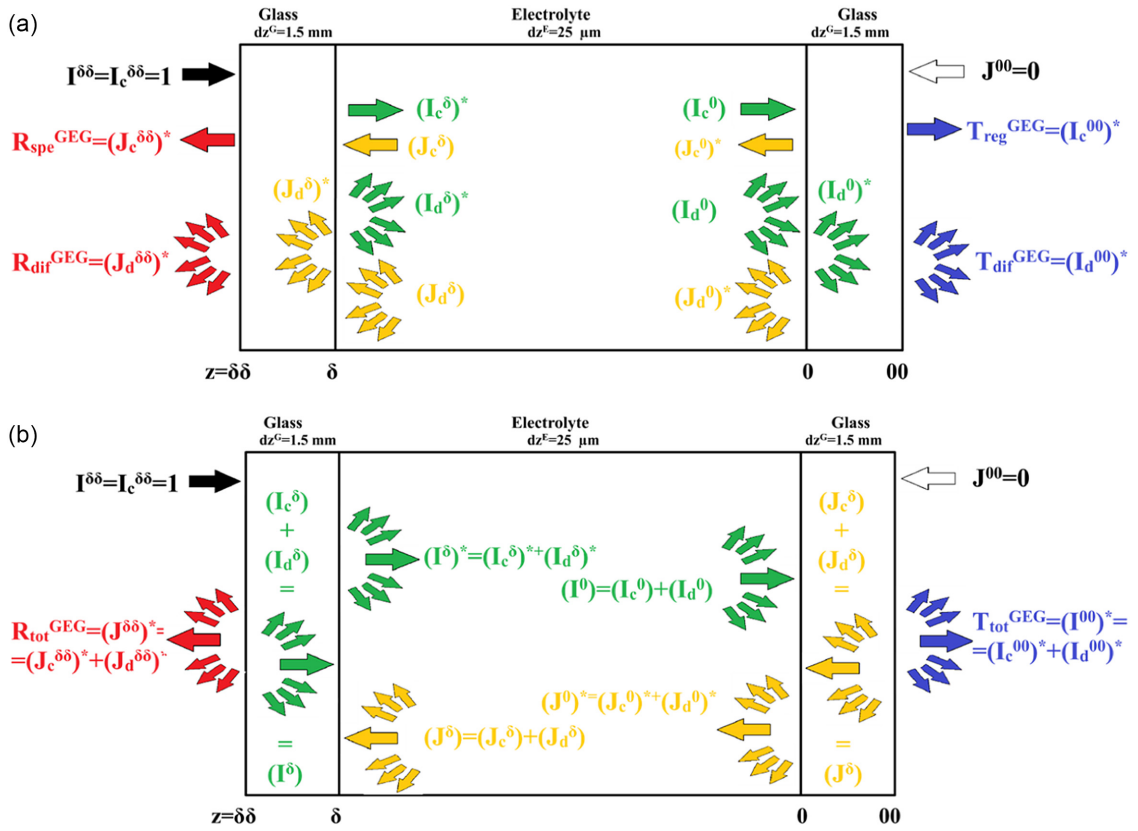

optical constants were obtained from the forward and backward *CDE*, once determined all collimated light intensities computed at the interfaces. This phenomenon, named the three-extinction matching requirement, was used for determining the rest of the new equations. Finally, the retrieved 4FM and 2FM parameters were used for plotting the thickness gradients of collimated, diffuse, and total light intensities, for forward and backward light senses.

2. Devices and Experimental Setup

Optical *T* and *R* measurements of the *GEG* sample were carried out in previous works [29] using a double-beam Perkin Elmer Lambda 950 spectrometer equipped with an integrating sphere, in the solar wavelength range (300–2500 nm), in steps of 5 nm. The sandwich structure of the *GEG* multilayer sample is shown in Figure 1. The sample was illuminated only by the front outer interface at $z = \delta\delta$, that is, with $I^{\delta\delta} = I_c^{\delta\delta} = 1$, and therefore $J^{00} = J_c^{00} + J_d^{00} = 0 = I_d^{\delta\delta}$, being the front and back inner interfaces at $z = \delta$ and $z = 0$ and with the front and back outer interfaces at $z = \delta\delta$ and $z = 00$, respectively. Figures 2 and 3 show the collimated and diffuse results for the 4FM [13, 14] solved parameters, respectively, obtained in Barrios Puerto [29] for the *GEG* sample. For the 2FM [12] solved parameters, Figure 3(b) shows the results obtained, comparing extrinsic (*S* and *K*) and intrinsic (α and β) scattering and absorption coefficients obtained. The sandwich structure of the *GEG* multilayer sample also appears in Figures 4, 5, and 6, not from left to right as in Figure 1, but from top to bottom, that is, the forward intensities pass to be descending from top to bottom, in contour diagrams (a), (b), and (c), and the backward intensities become ascending from bottom to top, in contour diagrams (d), (e), and (f), for collimated and diffuse light intensities gradients of Figures 4 and 5, and for total light intensities gradients of Figure 6.

The values of the light intensities shown in Figure 1 were computed at the interfaces using the intensities labeled with an asterisk (*), meaning that the intensity arrows do not end at the interface, but rather begins. These asterisked intensities follow the definition that at the interfaces light is neither scattered or absorbed but only transmitted or reflected. Therefore, T_{reg}^{GEG}, R_{spe}^{GEG}, T_{dif}^{GEG}, R_{dif}^{GEG}, T_{tot}^{GEG}, and R_{tot}^{GEG}, the collimated, diffuse, and total *T* and *R* measurements for the *GEG* sample are actually the values of the external intensities with an asterisk, divided by the incident intensity $I^{\delta\delta} = I_c^{\delta\delta} = 1$, that is, illuminating only by the front external interface side at $z = \delta\delta$ and none through the back external interface at $z = 00$ ($J^{00} = 0$). The rest of the intensities in Figure 1 are computed taking into account that light attenuation due to extinction occurs in the three substrate layers, that is, in the two outer front and back glass layers of thicknesses $dz^G = 1.5$ mm and especially in the inner electrolyte layer, of thickness $dz^E = 25$ μm, and not at the interfaces.

3. Theory

The theory presented below is developed for a three-substrate-layer assembly (Figure 1) with the electrolyte substrate (showing the main light scattering and absorption) placed inner and two glass substrate layers placed outer. Despite the *GEG* sample shows a low value of scattering and absorption, the equations developed in this section are thought to be valid for materials with any level of

Figure 2
Collimated-collimated (*cc*) transmittance and reflectance fittings and measurements of glass (G) and glass/electrolyte/glass (*GEG*) samples: (a) Regular transmittance and (b) specular reflectance. Comparison of extinction coefficients retrieved with collimated differential equations and with matrix form for glass (c) and electrolyte (d) substrate layers

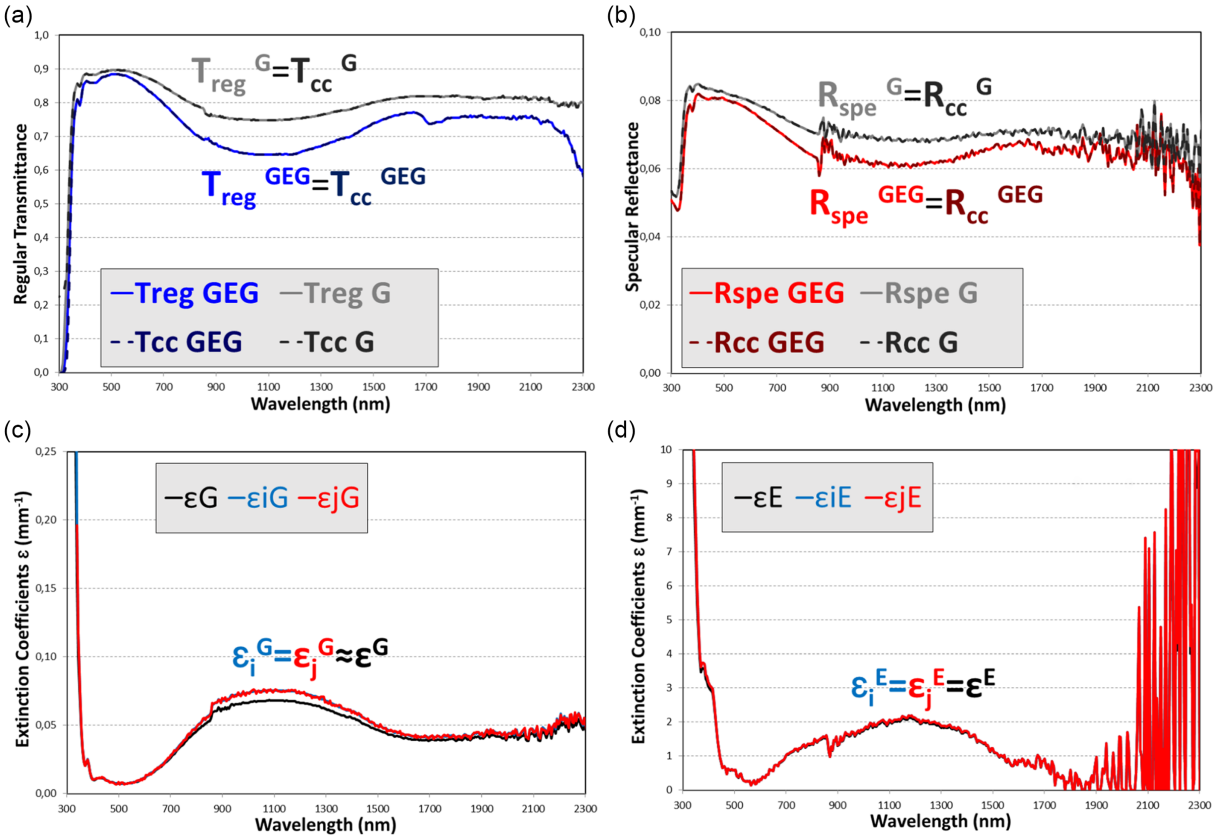

scattering and absorption. ACP (ξ) and FSR (σ) parameters and ε, α, and β coefficients retrieved from the *CDE* and the *DDE* of 4FM [13, 14] were first used in Barrios Puerto [29], being detailed in this section. The new equations for S and K coefficients were derived from the TDE of 2FM [12] for the multilayer *GEG* sample. Contrary to standard solutions of 4FM [14] and 2FM [12], the current solutions show a dependence of the extrinsic parameters on the intrinsic parameters, that is, S, $K = f(\alpha, \beta, \xi, \sigma)$. However, instead of one ACP and one FSR parameters, ACP will be two parameters ($ACP^i = \xi^i$ and $ACP^j = \xi^j$), depending on forward and backward light senses, and FSR will be four parameters ($FSR_c{}^i = \sigma_c{}^i$, $FSR_c{}^j = \sigma_c{}^j$, $FSR_d{}^i = \sigma_d{}^i$, and $FSR_d{}^j = \sigma_d{}^j$), depending on forward and backward light senses and also depending on collimated and diffuse light components. Besides, FSR and backward scattering ratio (BSR) are complementary, that is, $\sigma^i = 1 - \sigma^j$, for collimated and for diffuse flux, that is, $\sigma_c{}^i = 1 - \sigma_c{}^j$ and $\sigma_d{}^i = 1 - \sigma_d{}^j$. This section begins with the determination of the optical constants of the inner electrolyte layer, used to compute collimated and diffuse light intensities, which added are the total light intensities, required in the three systems of differential equations, *CDE* and *DDE* of 4FM [13, 14] and TDE of 2FM [12].

3.1. Optical constants of outer glass and inner electrolyte layer with matrices

Complex refractive index or optical constants (n and κ) of a material is shown in Equation (1). At an interface between outside (o) and inside (i) media, Fresnel transmission (τ) and reflection (ρ) coefficients at normal incidence, for S and P polarized light, are shown in Equations (2) to (5). Interface transmittance (t) and interface reflectance (r) are computed using Equations (6) and (7), respectively, being $X = S, P$, for both polarization of light, multiplying τ and ρ coefficients by its conjugated:

$$n' = n - i\kappa \tag{1}$$

$$\tau_{oi}{}^{S} = \frac{2n_o'}{n_o' + n_i'} \tag{2}$$

$$\rho_{oi}{}^{S} = \frac{n_o' - n_i'}{n_o' + n_i'} \tag{3}$$

$$\tau_{oi}{}^{P} = \frac{2n_o'}{n_o' + n_i'} \tag{4}$$

$$\rho_{oi}{}^{P} = \frac{n_i' - n_o'}{n_o' + n_i'} \tag{5}$$

$$t_{oi}^{X} = \mathrm{Re}\left(\frac{n_i'}{n_o'}\right) \cdot |\tau_{oi}^{X}|^2 = \mathrm{Re}\left(\frac{n_i'}{n_o'}\right) \cdot \tau_{oi}^{X} \cdot \hat{\tau}_{oi}^{X} \tag{6}$$

$$r_{oi}^{X} = |r_{oi}^{X}|^2 = \rho_{oi}^{X} \cdot \hat{\rho}_{oi}^{X} \tag{7}$$

Figure 3

(a) Diffuse transmittance and reflectance measurements of glass/electrolyte/glass (*GEG*) sample (error of calibration of the spectrometer detector at 900 nm), (b) Intrinsic and extrinsic scattering (α) and absorption (β) coefficients, (c) Forward scattering ratio ($FSR = \sigma$) for collimated and diffuse, forward (i) and backward (j) light intensities, light intensities, and (d) Average crossing parameter ($ACP = \xi$) for (i) and (j) light intensities

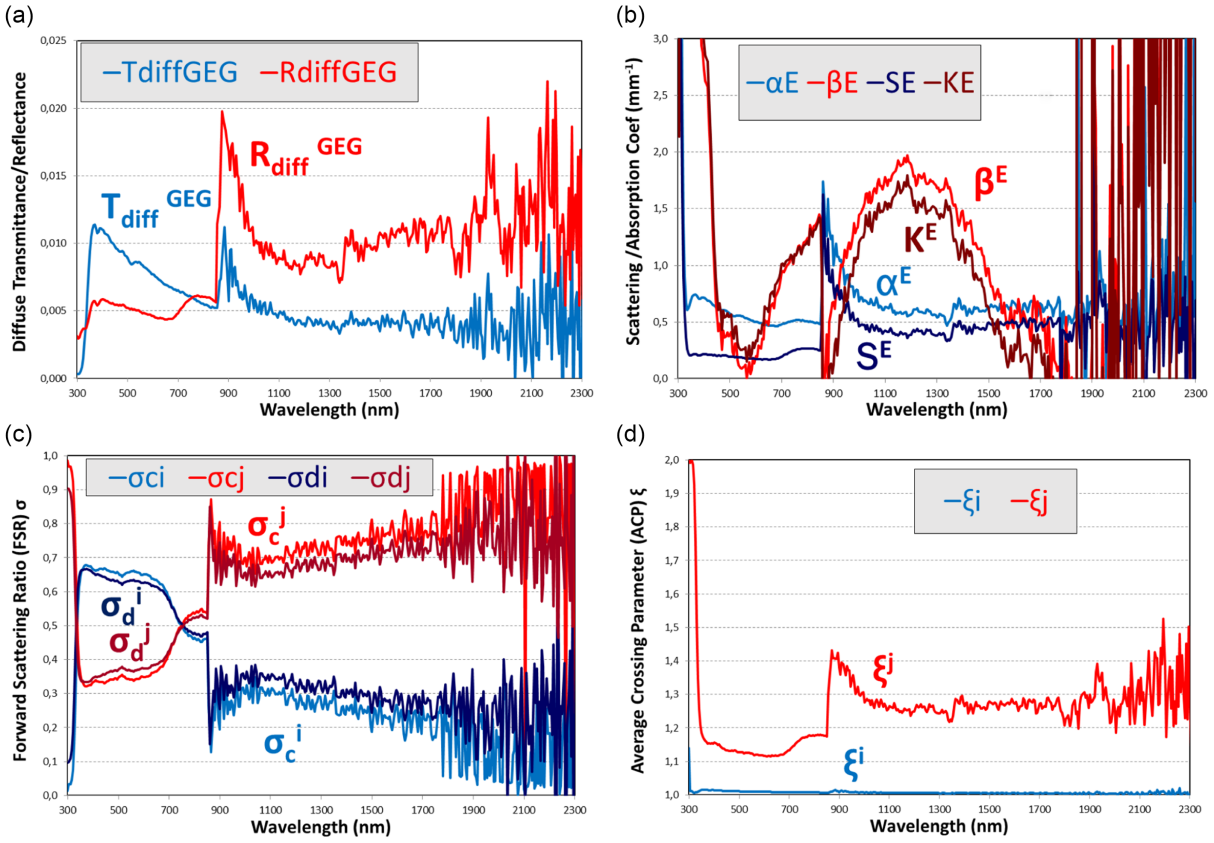

Interface matrix M_{oi} of Equation (8) using t_{oi} and r_{oi} parameters (i.e., the mean of two S & P polarized t and r) relates I_o & J_o and I_i & J_i, that is, the radiation intensity propagating forward (I) and backward (J) from an interface in the direction from the outside ("o") medium to the inside ("i") medium:

$$\begin{bmatrix} I_o \\ J_o \end{bmatrix} = \begin{bmatrix} \frac{1}{t_{oi}} & \frac{-r_{io}}{t_{oi}} \\ \frac{r_{oi}}{t_{oi}} & t_{io} - \frac{r_{io}r_{oi}}{t_{oi}} \end{bmatrix} \cdot \begin{bmatrix} I_i \\ J_i \end{bmatrix} = M_{oi} \cdot \begin{bmatrix} I_i \\ J_i \end{bmatrix} \tag{8}$$

Substrate layer matrix N_s: The extinction attenuation factor τ_c of a thick layer or substrate describing the reduction in intensity of radiation of wavelength $\lambda_n = \lambda/n$, from an initial value I_1 to the final value I_2 as it traverses the substrate layer of thickness d, is shown in Equation (9). Substrate layer matrix N_s describing the attenuation of a wave, as it traverses the medium within the substrate layer from initial (1) to final (2) positions, is shown in Equation (10). Matrix multiplication: Interface matrix and substrate layer matrix are used in two samples, that is, the glass sample, with a single substrate layer, for determining n^G and κ^G, and the *GEG* sample, with three substrate layers, for determining n^E and κ^E:

$$\tau_c = \frac{I_2}{I_1} = exp\left(-\frac{4\pi\kappa}{\lambda_n}d\right) = exp\left(-\frac{4\pi\kappa n}{\lambda}d\right) \tag{9}$$

$$\begin{bmatrix} I_s(1) \\ J_s(1) \end{bmatrix} = \begin{bmatrix} \frac{1}{\tau_c} & 0 \\ 0 & \tau_c \end{bmatrix} \cdot \begin{bmatrix} I_s(2) \\ J_s(2) \end{bmatrix} = N_s \cdot \begin{bmatrix} I_s(2) \\ J_s(2) \end{bmatrix} \tag{10}$$

Glass sample: Computing the substrate layer matrix between the two o-G and G-i interface matrices is shown in Equation (11). When illuminating only from the outside medium ("o") in the forward (I) direction, $I_o = 1$ and $J_i = 0$. Then, Equation (11) becomes Equation (12) and the forward intensity of the inside medium (I_i) and the backward intensity of the outside medium (J_o) are related to $T_{cc}{}^G$ and $R_{cc}{}^G$, respectively, that is, the T and R of an outside-glass medium interface matrix (M_{oG}), a glass layer matrix (N_G), and an inside-glass medium interface matrix (M_{Gi}):

$$\begin{bmatrix} I_o \\ J_o \end{bmatrix} = M_{oG} \cdot N_G \cdot M_{Gi} \cdot \begin{bmatrix} I_i \\ J_i \end{bmatrix} \tag{11}$$

$$\begin{bmatrix} 1 \\ R_{cc}^G \end{bmatrix} = M_{oG} \cdot N_G \cdot M_{Gi} \cdot \begin{bmatrix} T_{cc}^G \\ 0 \end{bmatrix} \tag{12}$$

GEG sample: Two outer interface matrixes (M_{oG} and M_{Gi}), two inner interface matrixes (M_{GE} and M_{EG}), two outer layer matrixes (N_G), and one inner layer matrix (N_E) are required for the *GEG* sample in order to calculate the electrolyte optical constants n^E and κ^E by fitting $T_{cc}{}^{GEG}$ and $R_{cc}{}^{GEG}$ to $T_{reg}{}^{GEG}$ and $R_{spe}{}^{GEG}$ measurements,

Figure 4

Collimated light intensities gradients of a glass/electrolyte/glass (*GEG*) sample. (a), (b), and (c) Forward light decreasing. (d), (e), and (f) Backward light decreasing. (a) and (f) Top glass outer layer. (b) and (f) Inner electrolyte layer. (c) and (d) Bottom glass outer layer

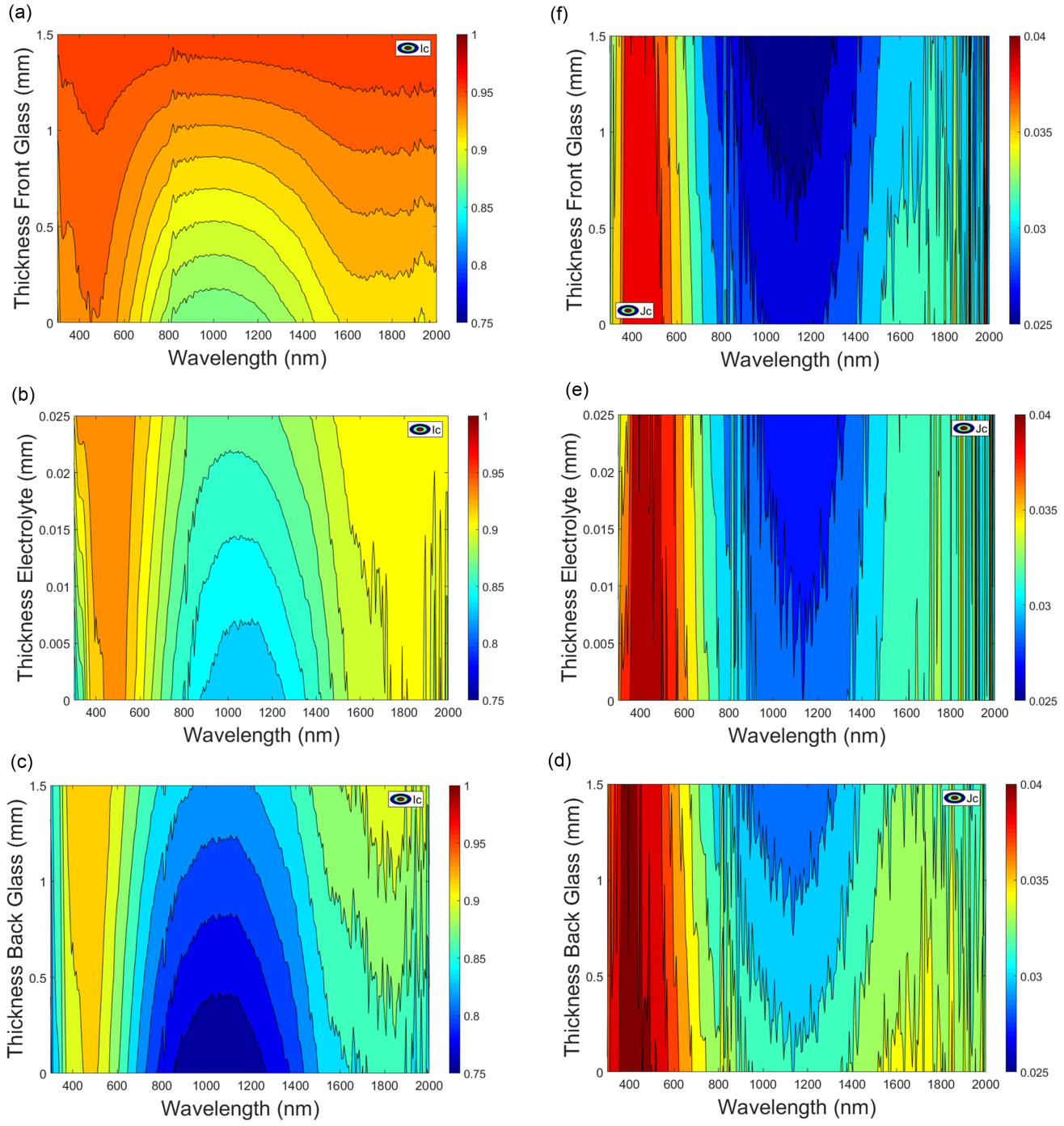

respectively. Hence, four interface matrices (M_{oG}, M_{GE}, M_{EG}, and M_{Gi}) and three layers matrices (N_G, twice, for front and back glass layers, and N_E) are observed in Equation (13):

$$\begin{bmatrix} 1 \\ R_{cc}^{GEG} \end{bmatrix} = M_{oG} \cdot N_G \cdot M_{GE} \cdot N_E \cdot M_{EG} \cdot N_G \cdot M_{Gi} \cdot \begin{bmatrix} T_{cc}^{GEG} \\ 0 \end{bmatrix} \quad (13)$$

Once glass and electrolyte optical constants are determined using matrix formulation of previous section by using Equations (12) and (13), respectively, collimated and diffuse light intensities are computed to be used in *CDE* and *DDE* of 4FM [13, 14].

3.2. Collimated and diffuse differential equations of 4FM

Showing a symmetrical behavior for forward and backward light senses, Equations (14) and (15) are the *CDE* [13, 14] that were used to obtain the forward and backward extinction coefficients ε_i and ε_j of the inner electrolyte layer of the *GEG*

Figure 5

Diffuse light intensities gradients of a glass/electrolyte/glass (*GEG*) sample. (a), (b), and (c) Forward light increasing. (d), (e), and (f) Backward light increasing. (a) and (f) Front glass outer layer. (b) and (f) Inner electrolyte layer. (c) and (d) Back glass outer layer

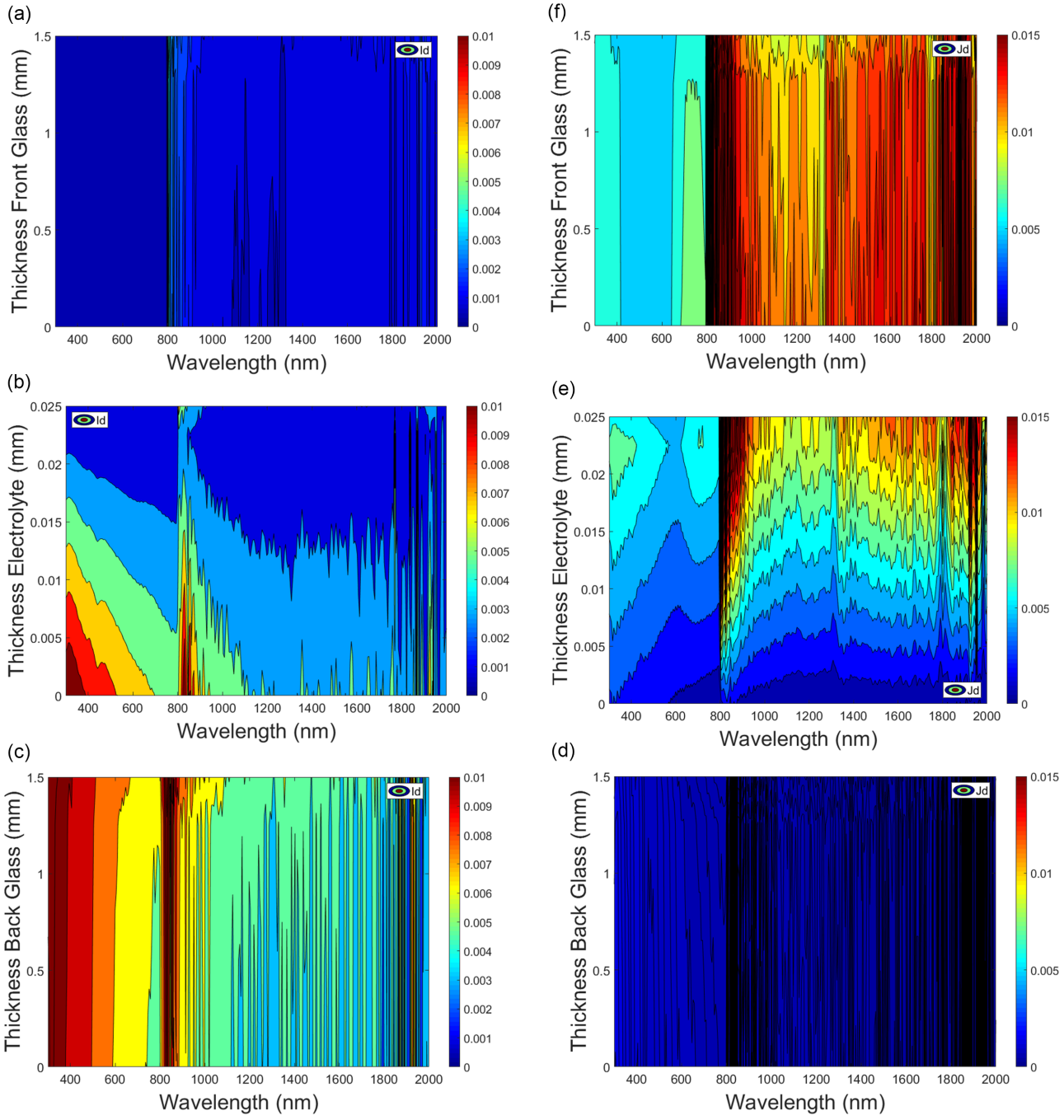

sample. In order to obtain all light intensities appearing at Equations (14) and (15), the following procedure from the outside to the inside of the sample should be carried out. Since $I_c^{\delta\delta} = 1$ and $J_c^{00} = 0$ in Figure 1, I_c^{00} and $J_c^{\delta\delta}$ are calculated from Equations (16) and (17) for the regular T and the specular R or collimated components, respectively. Hence, $T_{reg}{}^{GEG} = (I_c^{00})^*$ and $R_{spe}{}^{GEG} = (J_c^{\delta\delta})^*$. Then, I_c^{δ} and J_c^{0} are calculated with Equations (18) and (19), respectively. The system of Equations (20) and (21) was solved for I_c^{0} and J_c^{δ} in Equations (22) and (23), respectively. Collimated light intensities with asterisk $(I_c^{\delta})^*$ and $(J_c^{0})^*$ of Equations (14) and (15) are computed with Equations (24) and (25), respectively. Extinction coefficients for glass and electrolyte substrate layers ε^G and ε^E are given in Equation (26) and used to compute collimated attenuations $\tau_c{}^G$ and $\tau_c{}^E$ with Equation (27):

$$\frac{dI_c}{dz} = \frac{(I_c^{\delta})^* - (I_c^{0})}{dz^E} = \varepsilon_i \cdot (I_c^{\delta})^* \tag{14}$$

$$\frac{dJ_c}{dz} = \frac{(J_c^{\delta}) - (J_c^{0})^*}{dz^E} = -\varepsilon_j \cdot J_c^{\delta} \tag{15}$$

$$T_{reg}{}^{GEG} = (1 - r_c^G) \cdot I_c^{00} \tag{16}$$

Figure 6
Total light intensities gradients of a glass/electrolyte/glass (*GEG*) sample. (a), (b), and (c) Forward light decreasing. (d) and (f) Backward light decreasing and (e) increasing. (a) and (f) Front glass outer layer. (b) and (f) Inner electrolyte layer. (c) and (d) Back glass outer layer

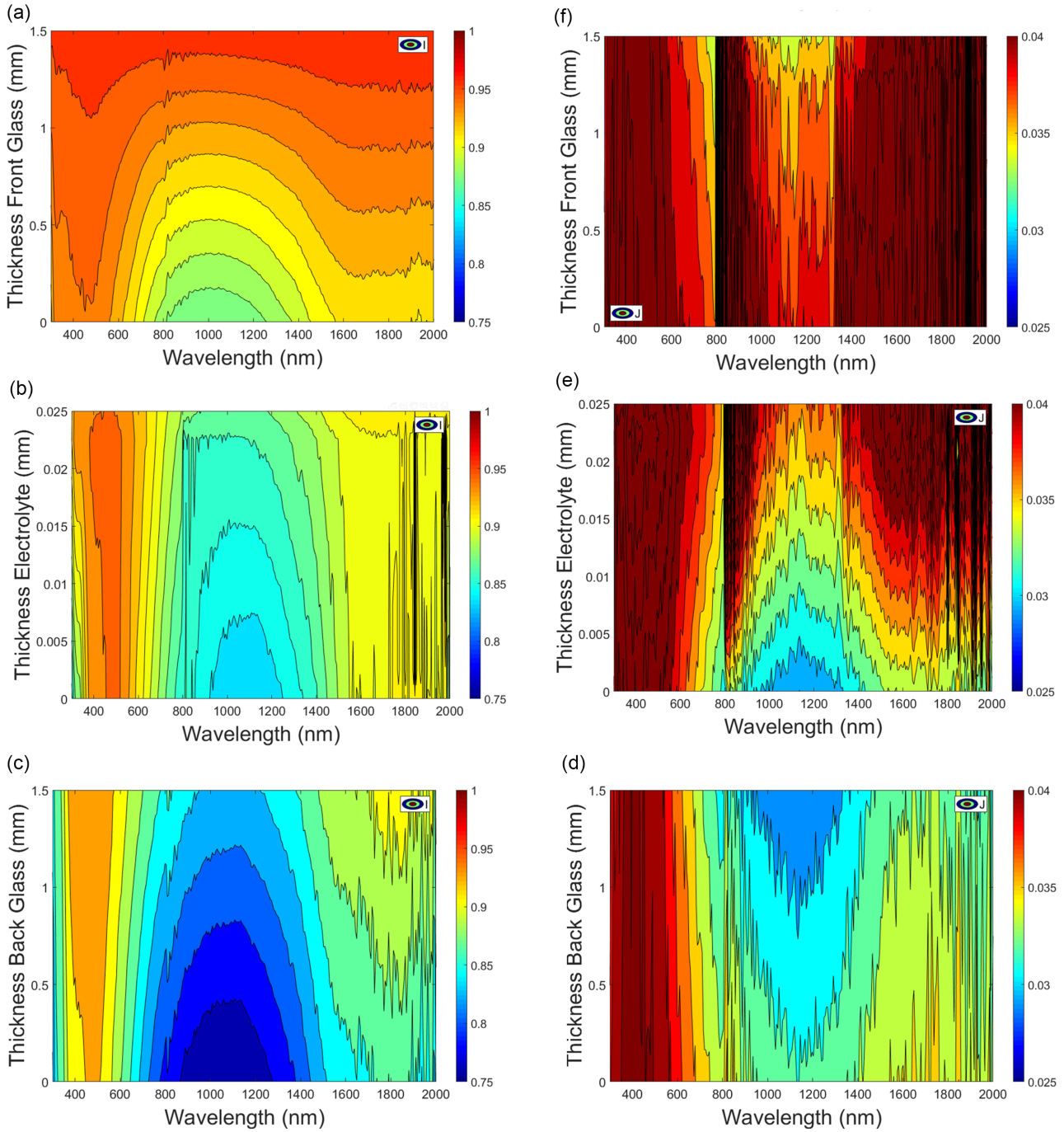

$$R_{spe}{}^{GEG} = r_c^G + (1 - r_c^G) \cdot J_c^{\delta\delta} \tag{17}$$

$$I_c^{\delta} = \{(1 - r_c^G) + r_c^G \cdot J_c^{\delta\delta}\} \cdot \tau_c^G \tag{18}$$

$$J_c^0 = r_c^G \cdot I_c^{00} \cdot \tau_c^G \tag{19}$$

$$I_c^0 = \{(1 - r_c^{GE}) \cdot I_c^{\delta} + r_c^{GE} \cdot J_c^{\delta}\} \cdot \tau_c^E \tag{20}$$

$$J_c^{\delta} = \{(1 - r_c^{GE}) \cdot J_c^0 + r_c^{GE} \cdot I_c^0\} \cdot \tau_c^E \tag{21}$$

$$I_c^0 = \tau_c^E \cdot \tau_c^G \cdot \frac{(1 - r_c^G) \cdot (1 - r_c^{GE}) + I_c^{00} \cdot r_c^G \cdot r_c^{GE} \cdot (1 - r_c^{GE}) \cdot \tau_c^E + J_c^{\delta\delta} \cdot r_c^G \cdot (1 - r_c^{GE})}{1 - (r_c^{GE} \cdot \tau_c^E)^2} \tag{22}$$

$$J_c^{\delta} = \tau_c^E \cdot \tau_c^G \cdot \frac{r_c^{GE} \cdot (1 - r_c^G) \cdot (1 - r_c^{GE}) \cdot \tau_c^E + I_c^{00} \cdot r_c^G \cdot (1 - r_c^{GE}) + J_c^{\delta\delta} \cdot r_c^G \cdot r_c^{GE} \cdot (1 - r_c^{GE}) \cdot \tau_c^E}{1 - (r_c^{GE} \cdot \tau_c^E)^2} \tag{23}$$

$$(I_c^{\delta})^* = (1 - r_c^{GE}) \cdot I_c^{\delta} + r_c^{GE} \cdot J_c^{\delta} \tag{24}$$

$$(J_c^0)^* = (1 - r_c^{GE}) \cdot J_c^0 + r_c^{GE} \cdot I_c^0 \tag{25}$$

$$\varepsilon^X = \frac{4 \cdot \pi \cdot \kappa^X}{\lambda_{n^X}} = \frac{4 \cdot \pi \cdot \kappa^X \cdot n^X}{\lambda} = \alpha^X + \beta^X; X = G, E \tag{26}$$

$$\tau_c^X = e^{-\varepsilon^X \cdot dz^X}; X = G, E \tag{27}$$

As observed in Equation (9) for determining τ_c, the Equation (26) can be used to verify that the wavelength (λ) must be $\lambda_n = \lambda/n$ instead of λ, that is, lower wavelength than that of empty space or air, since $n \geq 1$. Taking this into account, the forward and backward light extinction coefficients ε_i and ε_j were obtained according to the *CDE* in Equations (14) and (15) and compared with ε^X from Equation (26) when $x = E$ (electrolyte), turning out to be equal when using the sandwich structure of Figure 1, suitable for the measured *GEG* sample, with three substrate layers. Then, in the same way, α and β intrinsic coefficients can be obtained by means of the *DDE*, that is, from Equations (28) and (29). In order to obtain all light intensities appearing at the *DDE* in Equations (28) and (29), as at the *CDE* in Equations (14) and (15), the following procedure from the outside to the inside of the sample should be carried out. Since $I_d^{\delta\delta} = J_d^{00} = 0$ in Figure 1, I_d^{00} and $J_d^{\delta\delta}$ are calculated from Equations (30) and (31), for the diffuse T and R components, respectively. Hence, $T_{dif}^{GEG} = (I_d^{00})^*$ and $R_{dif}^{GEG} = (J_d^{\delta\delta})^*$. Then, I_d^{δ} and J_d^{0} are calculated with Equations (32) and (33), being I_d^0 and J_d^δ with Equations (34) and (35). Diffuse light intensities with asterisk $(I_d^\delta)^*$ and $(J_d^0)^*$ of Equations (28) and (29) are computed with Equations (36) and (37), respectively. Then, r_d^G and r_d^{GE} are computed using the Equation (38) [19] with $m = n_2/n_1$, being $n_1 < n_2$, that is, when traveling from the faster to the slower medium. As with r_c, r_d also shows a bidirectional behavior when integrating up to θ_c [20–22]. The collimated attenuation of glass (τ_c^G) was computed with Equation (27) for $X = G$ (glass) and the diffuse attenuation of glass (τ_d^G) was computed with Equation (39), integrating the extinction attenuation of light, inside the glass layer, up to θ_c:

$$\frac{dI_d}{dz} = \frac{(I_d^\delta)^* - I_d^0}{dz^E} = -(I_c^\delta)^* \sigma_c^j \alpha - J_c^\delta \sigma_c^i \alpha - J_d^\delta \xi^j \sigma_d^i \alpha + \left(\xi^i \beta + \xi^i \sigma_d^j \alpha\right) \tag{28}$$

$$\frac{dJ_d}{dz} = \frac{J_d^\delta - (J_d^0)^*}{dz^E} = J_c^\delta \sigma_c^i \alpha + (I_c^\delta)^* \sigma_c^j \alpha + (I_d^\delta)^* \xi^i \sigma_d^j - J_d^\delta \left(\xi^j \beta + \xi^j \sigma_d^i \alpha\right) \tag{29}$$

$$T_{dif}^{GEG} = \left(1 - r_d^G\right) \cdot I_d^{00} \tag{30}$$

$$R_{dif}^{GEG} = \left(1 - r_d^G\right) \cdot J_d^{\delta\delta} \tag{31}$$

$$I_d^\delta = \left(I_d^{\delta\delta}\right)^* \cdot \tau_d^G = r_d^G \cdot J_d^{\delta\delta} \cdot \tau_d^G \tag{32}$$

$$J_d^0 = \left(J_d^{00}\right)^* \cdot \tau_d^G = r_d^G \cdot I_d^{00} \cdot \tau_d^G \tag{33}$$

$$I_d^0 = \frac{(I_d^0)^* - r_d^{GE} \cdot J_d^0}{1 - r_d^{GE}} = \frac{\frac{I_d^{00}}{\tau_d^G} - r_d^{GE} \cdot J_d^0}{1 - r_d^{GE}} \tag{34}$$

$$J_d^\delta = \frac{(J_d^\delta)^* - r_d^{GE} \cdot I_d^\delta}{1 - r_d^{GE}} = \frac{\frac{J_d^{\delta\delta}}{\tau_d^G} - r_d^{GE} \cdot I_d^\delta}{1 - r_d^{GE}} \tag{35}$$

$$\left(I_d^\delta\right)^* = \left(1 - r_d^{GE}\right) \cdot I_d^\delta + r_d^{GE} \cdot J_d^\delta \tag{36}$$

$$\left(J_d^0\right)^* = \left(1 - r_d^{GE}\right) \cdot J_d^0 + r_d^{GE} \cdot I_d^0 \tag{37}$$

$$f(m) = \frac{1}{2} + \frac{(m-1)(3m+1)}{6(m+1)^2} + \left[\frac{m^2(m^2-1)^2}{(m^2+1)^2}\right] \ln\frac{m-1}{m+1} - -\frac{2m^2(m^2-2m-1)}{(m^2+1)(m^4-1)} + \left[\frac{8m^4(m^4+1)}{(m^2+1)(m^4-1)^2}\right] \ln(m) \tag{38}$$

$$\tau_d^G = \int_0^{\theta_C} e^{-\frac{\varepsilon^G \cdot dz^G}{\cos\theta}} \cdot d\theta \tag{39}$$

$$\xi = 1 + \frac{I_d^0 + J_d^\delta}{I_c^0 + I_d^0 + J_c^\delta + J_d^\delta} \tag{40}$$

Once calculated all light intensities of the system of the *DDE* in Equations (28) and (29) in Barrios Puerto [29] and based on the Equation (40) used for ACP in Barrios et al. [22] as the fifth equation, intuitive expressions were proposed: Equations (41) and (42), for the two ACPs (ξ^i and ξ^j) and Equations (43) and (44), for the two FSR parameters for diffuse light intensities (σ_d^i and σ_d^j), in both light senses, that is, FSR and complementary BSR, that is, $\sigma_x^i = 1 - \sigma_x^j$, $x = c,d$. The complementary of σ_d^i and σ_d^j can be easily observed in Equations (43) and (44). Now the system of the *DDE* in Equations (28) and (29) can be solved for α and σ_c^i in Equations (45) and (46), respectively. According to Equation (26), for the electrolyte layer, intrinsic absorption coefficient β is calculated subtracting extinction and intrinsic scattering coefficients:

$$\xi^i = 1 + \frac{I_d^0}{I_c^0 + I_d^0} \tag{41}$$

$$\xi^j = 1 + \frac{J_d^\delta}{J_c^\delta + J_d^\delta} \tag{42}$$

$$\sigma_d^i = \frac{I_d^0}{I_d^0 + J_d^\delta} \tag{43}$$

$$\sigma_d^j = \frac{J_d^\delta}{I_d^0 + J_d^\delta} \tag{44}$$

$$\alpha = \frac{I_d^0 - (I_d^\delta)^* - (J_d^0)^* + J_d^\delta + \langle \xi^i \cdot (I_d^\delta)^* + \xi^j \cdot J_d^\delta \rangle \cdot \varepsilon^E \cdot dz^E}{dz^E \cdot \langle (I_c^\delta)^* + J_c^\delta + \xi^i \cdot (I_d^\delta)^* + \xi^j \cdot J_d^\delta \rangle} \tag{45}$$

$$\sigma_c^i = \frac{A + B1 + B2 + C}{D} \tag{46}$$

$$A = \left[(I_c^\delta)^* + J_c^\delta + \xi^j J_d^\delta\right] \cdot \left[I_d^0 - (I_d^\delta)^*\right]$$

$$B1 = \xi^i (I_d^\delta)^* \left\langle (J_d^0)^* - J_d^\delta + [(I_c^\delta)^* + J_c^\delta] \varepsilon^E dz^E \right\rangle$$

$$B2 = \xi^i (I_d^\delta)^* \sigma_d^j \langle I_d^0 + J_d^\delta - (J_d^0)^* - (I_d^\delta)^* + + \varepsilon^E dz^E \left[\xi^i (I_d^\delta)^* + \xi^j J_d^\delta\right] \rangle$$

$$C = \xi^j \sigma_d^i J_d^\delta \left\langle (I_d^\delta)^* + (J_d^0)^* - I_d^0 - J_d^\delta + + \varepsilon^E dz^E \left[\xi^j J_d^\delta - \xi^i (I_d^\delta)^*\right] \right\rangle$$

$$D = [(I_c^\delta)^* + J_c^\delta] I_d^0 - (I_d^\delta)^* - (J_d^0)^* + J_d^\delta + + \varepsilon^E dz^E \left[\xi^i (I_d^\delta)^* + \xi^j J_d^\delta\right]$$

3.3. Total differential equations of 2FM

Considering that the TDE in Equations (47) and (48) of the 2FM [12] can be computed as the sum of the *CDE* – Equations (14) and

(15) − and the *DDE* − Equations (28) and (29) − of the 4FM [13, 14], S and K can be solved as a function of α, β, ξ, and σ parameters. Values of collimated and diffuse inner light intensities, that is, $I_c^{\,0}$, $I_d^{\,0}$, $(I_c^{\,\delta})^*$, $(I_d^{\,\delta})^*$, $J_c^{\,\delta}$, $J_d^{\,\delta}$, $(J_c^{\,0})^*$, and $(J_d^{\,0})^*$, are computed from Equations (22), (34), (24), (36), (23), (35), (25), and (37), respectively. Note that since TDE = *CDE* + *DDE*, Equation (47) is equal to Equation (14) plus Equations (28) and Equation (48) is equal to Equation (15) plus Equation (29). Then, solving S and K, Equations (49) and (50) are obtained as function of intrinsic parameters and collimated and diffuse light intensities related to 4FM retrieved in the previous section, that is, α, β, ξ^x, $\sigma_Y^{\,x}$, $X_Y^{\,Z}$, and $(X_Y^{\,Z})^*$, being $X = I,J$, $Y = c,d$, and $Z = 0,\delta$. Since light at interfaces can only be transmitted or reflected, collimated and diffuse interface transmittance (t_c and t_d) are complementary to r_c and r_d, respectively (i.e., $t_c = 1-r_c$ and $t_d = 1-r_d$). Besides, due to the θ_c used as limit of integration for r_d, they are bidirectional:

$$\frac{dI}{dz} = \frac{(I_c^{\delta})^* + (I_d^{\delta})^* - I_c^0 - I_d^0}{dz^E} = (S+K)\cdot\left((I_c^{\delta})^* + (I_d^{\delta})^*\right) - S\cdot\left(J_c^{\delta} + J_d^{\delta}\right) \tag{47}$$

$$\frac{dJ}{dz} = \frac{(J_c^{\delta}) + J_d^{\delta} - (J_c^0)^* - (J_d^0)^*}{dz^E} = -(S+K)\cdot\left(J_c^{\delta} + J_d^{\delta}\right) + S\cdot\left((I_c^{\delta})^* + (I_d^{\delta})^*\right) \tag{48}$$

$$S = \frac{S_{IJ}^{cd} + S_{IJ}^{dc} + S_{II}^{cc} + S_{JJ}^{cc} + S_{JJ}^{dd} + S_{IJ}^{dd} + S_{II}^{cd} + S_{JJ}^{cd} + S_{II}^{dd} + S_{JJ}^{cc}}{D_S \cdot D_{SK}} \tag{49}$$

$$D_S = (I_c^{\delta} - J_c^{\delta})t_c^{GE} + (I_d^{\delta} - J_d^{\delta})t_d^{GE}$$

$$D_{SK} = I_c^{\delta}t_c^{GE} + I_d^{\delta}t_d^{GE} + J_c^{\delta}r_c^{GE} + J_d^{\delta}r_d^{GE} + J_c^{\delta} + J_d^{\delta}$$

$$S_{IJ}^{cd} = I_c^{\delta}J_d^{\delta}t_c^{GE}\cdot\left[\alpha\left(1 + \xi^i\sigma_d^{\,j}r_d^{GE} - \xi^j\sigma_d^{\,i} - \sigma_c^{\,j}t_d^{GE}\right) + \beta(1-\xi^j)\right]$$

$$S_{IJ}^{dc} = -I_d^{\delta}J_c^{\delta}t_d^{GE}\cdot\left\langle\alpha\left[1 - \left(\sigma_c^{\,j} + \xi^i\sigma_d^{\,j}\right)(1 + r_c^{GE})\right] + \beta[1-\xi^i]\right\rangle$$

$$S_{II}^{cc} = (I_c^{\delta})^2\alpha\sigma_c^{\,j}[1 + r_c^{GE}(r_c^{GE} - 2)]$$

$$S_{JJ}^{cc} = (J_c^{\delta})^2\alpha\left[\sigma_c^{\,j}(r_c^{GE})^2 - \sigma_c^{\,i}\right]$$

$$S_{JJ}^{dd} = (J_d^{\delta})^2 r_d^{GE} \cdot\left\langle\left[\beta(\xi^i - \xi^j) - \alpha\left(\xi^j\sigma_d^{\,i} - \xi^i\sigma_d^{\,j}r_d^{GE}\right)\right] - \alpha\left(\xi^j\sigma_d^{\,i} - \xi^i\sigma_d^{\,j}r_d^{GE}\right)\right\rangle$$

$$S_{IJ}^{dd} = I_d^{\delta}J_d^{\delta} \cdot\left\langle\alpha\left[\xi^i\sigma_d^{\,j}\left(1 + r_d^{GE} - 2(r_d^{GE})^2\right) - \xi^i\sigma_d^{\,i}t_d^{GE}\right] + \beta\left[(\xi^i - \xi^j)t_d^{GE}\right]\right\rangle$$

$$S_{II}^{cd} = I_c^{\delta}I_d^{\delta}t_c^{GE}t_d^{GE}\alpha\left[\sigma_c^{\,j} + \xi^i\sigma_d^{\,j}\right]$$

$$S_{JJ}^{cd} = J_c^{\delta}J_d^{\delta}\left\{\alpha\cdot\left[\left(r_c^{GE} - r_d^{GE}\right)\left(1 - \sigma_c^{\,j}\right) - \Phi\right] + \beta\cdot\left[r_c^{GE}(1-\xi^i) - r_d^{GE}(1-\xi^i)\right]\right\}$$

$$\Phi = \sigma_c^{\,j}r_c^{GE}r_d^{GE} - \sigma_c^{\,i} - \left(\xi^i\sigma_d^{\,i} - \xi^i\sigma_d^{\,j}r_d^{GE}\right)(1 + r_c^{GE})$$

$$S_{II}^{dd} = (I_d^{\delta})^2\alpha\xi^i\left[1 + r_d^{GE}\sigma_d^{\,j}\left(r_d^{GE} - 2\right)\right]$$

$$K = \frac{K_I^c + K_J^c + K_I^d + K_J^d}{D_{SK}} \tag{50}$$

$$K_I^c = I_c^{\delta}t_c^{GE}\alpha\left(1 - 2\sigma_c^{\,j}\right) + \beta$$

$$K_J^c = J_c^{\delta}\alpha\left[t_c^{GE} - 2\sigma_c^{\,j}(1 + r_c^{GE}) + \beta t_c^{GE}\right]$$

$$K_I^d = I_d^{\delta}\beta\xi^i t_d^{GE}$$

$$K_J^d = J_d^{\delta}\beta\xi^j\left(1 + r_d^{GE}\right)$$

Note that collimated and diffuse asterisk outer light intensities in Figure 1(a), starting instead of finishing at the interfaces, correspond to collimated and diffuse measurements, that is, $T_{reg}^{\,GEG} = (I_c^{\,00})^*$, $R_{spe}^{\,GEG} = (J_c^{\,\delta\delta})^*$, $T_{dif}^{\,GEG} = (I_d^{\,00})^*$, and $R_{dif}^{\,GEG} = (J_d^{\,\delta\delta})^*$. Then, total T and R components of Figure 1(b) are calculated adding collimated and diffuse T and R components of Figure 1(a), respectively, that is, $T_{tot}^{\,GEG} = T_{reg}^{\,GEG} + T_{dif}^{\,GEG} = (I_c^{\,00})^* + (I_d^{\,00})^*$ and $R_{tot}^{\,GEG} = R_{spe}^{\,GEG} + R_{dif}^{\,GEG} = (J_c^{\,\delta\delta})^* + (J_d^{\,\delta\delta})^*$.

4. Results and Discussion

Optical constants were first obtained by a single fitting process from collimated T and R measured components, required for determining intrinsic and extrinsic parameters from the expressions of Section 3. Fitting T_{reg} and R_{spe} measurements to T_{cc} and R_{cc} Equations (12) and (13), respectively, for both G and *GEG* samples, are shown in Figure 2(a) and (b), respectively. A very small value for extinction coefficients ε is obtained for the glass substrate layer in Figure 2(c) compared with the value obtained for the electrolyte (E) substrate layer in Figure 2(d), that is, $\varepsilon^G << \varepsilon^E$. The slight difference between $\varepsilon_i^{\,G} = \varepsilon_j^{\,G} \approx \varepsilon^G$ obtained for the G layer from the *CDE* Equations (14) and (15) and from matrix form Equation (26) is related to the calibration of the used spectrometer. A perfect match is obtained for the E layer.

Measurements of T_{dif} and R_{dif} for the *GEG* sample are shown in Figure 3(a). Intrinsic scattering (α) and absorption (β) coefficients of the electrolyte layer were determined in Figure 3(b) from Equations (26) and (45), since $\beta = \varepsilon - \alpha$. FSR and BSR show small differences for collimated and diffuse light intensities ($\sigma_c^{\,i} \approx \sigma_d^{\,i}$ and $\sigma_c^{\,j} \approx \sigma_d^{\,j}$) in Figure 3(c). They were determined from Equations (43), (44), and (46), and knowing that $\sigma_c^{\,j} = 1 - \sigma_c^{\,i}$. A higher value of ACP for backward light, from Equation (42), than for forward light, from Equation (41), observed in Figure 3(d), is explained by a higher haze (H) or diffuse/total ratio in R than in T − in Figure 2(a), 2(b) and Figure 3(a) − or $H_R > H_T$, with $H_R = R_{dif}^{\,GEG}/R_{tot}^{\,GEG}$ and $H_T = T_{dif}^{\,GEG}/T_{tot}^{\,GEG}$. Extrinsic coefficients (S and K) for the inner electrolyte layer of the three layers *GEG* sample, computed from Equations (49) and (50), respectively, are observed in Figure 3(b), together with intrinsic coefficients (α and β).

The ultraviolet cutoff of the glass substrate layer, observed for both G and *GEG* samples, causes the abrupt drop observed in Figure 2(c) and (d) at the start of the spectrum, since almost no light is transmitted, with highly increasing of the extinction.

Collimated, diffuse, and total light intensities gradients are now obtained using the methods described in Section 3, that is, from extinction coefficients obtained from optical constants, and from the intrinsic scattering and absorption coefficients, using the two ACPs and the four FSRs, and from the extrinsic scattering and absorption coefficients, respectively. For collimated light intensities gradients, $(I_c^{\,\delta})^*$ and $J_c^{\,\delta}$ must be substituted by $(I_c^{\,Z})^*$ and $J_c^{\,Z}$ in *CDE* Equations (14) and (15), respectively, in order to compute collimated forward and backward light intensities at each point of the layer. Equations (51) and (52) are then used for this

task. As in *CDE* with $(I_c^{\delta})^*$ and J_c^{δ}, for diffuse light intensities gradients, $(I_d^{\delta})^*$ and J_d^{δ} must be substituted by $(I_d^{Z})^*$ and J_d^{Z} in Equations (45) and (46), respectively, which are the solutions of the *DDE* Equations (28) and (29), in order to compute diffuse forward and backward light intensities at each point of the layer. Equations (53) and (54) are then used for this task. Note that $(I_d^{Z})^*$ and J_d^{Z} also depend on $(I_c^{Z})^*$ and J_c^{Z} of Equations (51) and (52), respectively. For total light intensity gradients, TDE Equations (47) and (48) become Equations (55) and (56), where $I^0 = I_c^{\,0} + I_d^{\,0}$ and $(J^0)^* = (J_c^{\,0})^* + (J_c^{\,0})^*$, being $(I^Z)^* = (I_c^{Z})^* + (I_c^{Z})^*$ and $J^Z = J_c^{\,Z} + J_d^{\,Z}$ the unknowns, solved in Equations (57) and (58), respectively:

$$(I_c^Z)^* = \frac{I_c^0}{1 - \varepsilon^i \cdot Z} \tag{51}$$

$$J_c^Z = \frac{(J_c^o)^*}{1 + \varepsilon^j \cdot Z} \tag{52}$$

$$(I_d^Z)^* = -\frac{(A^I + B^I + C^I)}{D + E} \tag{53}$$

$$J_d^Z = -\frac{(A^J + B^J + C^J)}{D + E} \tag{54}$$

$$A^I = I_d^0\left\{\xi^i Z\left[\alpha\left(1 - \sigma_d^i\right) - \varepsilon\right] - 1\right\} + \; + \sigma_c^i \alpha Z\langle (I_c^Z)^* + J_c^Z\rangle$$

$$B^I = \xi^j \sigma_d^i \alpha Z\left\langle \left(J_d^0\right)^* + \alpha dz^E (I_c^{\delta})^*\right\rangle + + \xi^{-}\alpha^2 Z^2\left\langle \sigma_d^i J_c^Z - \sigma_c^i (I_c^Z)^*\right\rangle$$

$$C^I = \xi^j \sigma_c^i \alpha Z^2\langle \varepsilon (I_c^Z)^* - (\alpha + \varepsilon) J_c^Z\rangle$$

$$A^J = [1 + \xi^i Z(\varepsilon - \alpha)]\left(J_d^0\right)^* - \alpha Z[1 + + \xi^i \alpha Z]\langle (I_c^Z)^* + J_c^Z\rangle$$

$$B^J = \alpha Z\left\{\sigma_c^i\langle (I_c^Z)^* + J_c^Z\rangle + \xi^i \sigma_d^j\left\langle \left(J_d^0\right)^* - I_d^0\right\rangle\right\}$$

$$C^J = \alpha Z^2 \xi^i\left[\varepsilon(1 - \sigma_c^i) + \alpha\left(\sigma_d^j + \sigma_c^i\right)\right]\langle (I_c^Z)^* + J_c^Z\rangle$$

$$D = 1 + [(\xi^i - \xi^j)(1 - \varepsilon)]\alpha Z - \xi^i \xi^j Z^2(\alpha^2 + \varepsilon^2)$$

$$E = \alpha Z\left\{\left[\xi^j \sigma_d^i - \xi^i \sigma_d^j\right] + \xi^j \xi^i Z\left[\left(2 - \sigma_d^j - \sigma_d^i\right)\varepsilon + + \alpha\left(\sigma_d^i + \sigma_d^j\right)\right]\right\}$$

$$\frac{dI}{dz} = \frac{(I^Z)^* - I^0}{Z} = (S + K) \cdot (I^Z)^* - S \cdot J^Z \tag{55}$$

$$\frac{dJ}{dz} = \frac{J^Z - (J^0)^*}{Z} = -(S + K) \cdot J^Z + S \cdot (I^Z)^* \tag{56}$$

$$(I^Z)^* = \frac{I^0 \cdot [1 + (K + S) \cdot Z] - (J^0)^* \cdot S \cdot Z}{1 + Z^2 \cdot K \cdot (2 \cdot S - K)} \tag{57}$$

$$J^Z = \frac{(J^0)^* \cdot [1 - (K + S) \cdot Z] + I^0 \cdot S \cdot Z}{1 + Z^2 \cdot K \cdot (2 \cdot S - K)} \tag{58}$$

Collimated, diffuse, and total light intensities gradients of Figures 4, 5, and 6, respectively, were carried out computing nine inner light intensities values in steps of 2.5 μm, for the inner electrolyte layer, and five inner light intensities values, for front and back outer glass layers. Hence, for the electrolyte inner layer of 25 μm thickness, the inner light intensities were computed using Equations (51) to (58) for $z_0 = 0$, $z_1 = 2.5$ μm, $z_2 = 5$ μm, $z_3 = 7.5$ μm, $z_4 = 10$ μm, $z_5 = 12.5$ μm, $z_6 = 15$ μm, $z_7 = 17.5$ μm, $z_8 = 20$ μm, $z_9 = 22.5$ μm, and $z_{10} = 25$ μm $= dz^E$, being the light intensities at z_0 and z_{10} (placed at $z = 0$ and at $z = \delta$, respectively, in Figure 1), the light intensities at the extremes previously computed. For forward collimated and diffuse light intensities at the electrolyte layer, $I_c(z_0) = I_c^{\,0}$ and $I_d(z_0) = I_d^{\,0}$ using Equations (22) and (34), respectively, and $I_c(z_{10}) = (I_c^{\delta})^*$ and $I_d(z_{10}) = (I_d^{\delta})^*$, computed using Equations (24) and (36), respectively. For backward collimated and diffuse light intensities at the electrolyte layer, $J_c(z_0) = (J_c^{\,0})^*$ and $J_d(z_0) = (J_d^{\,0})^*$ using Equations (25) and (37), respectively, and $J_c(z_{10}) = J_c^{\,\delta}$ and $J_d(z_{10}) = J_d^{\,\delta}$, computed using Equations (23) and (35), respectively.

Forward and backward total light intensities were computed adding collimated and diffuse light intensities – $I(z_0) = I_c(z_0) + I_d(z_0) = (I_c^{\delta})^*$, $I(z_{10}) = I_c(z_{10}) + I_d(z_{10}) = I_c^{\,0}$, $J(z_0) = J_c(z_0) + J_d(z_0) = J_c^{\,\delta}$, and $J(z_{10}) = J_c(z_{10}) + J_d(z_{10}) = (J_c^{\,0})^*$. Then, for the front and back outer glass layers, both of 1.5 mm thicknesses, the five inner light intensities were computed (from ε^G previously calculated in Figure 2(c) using Equation (26) for $X = G$) using Equations (51) and (52) for the collimated values, at $z_1 = 0.25$ mm, $z_2 = 0.5$ mm, $z_3 = 0.75$ mm, $z_4 = 1$ mm, and $z_5 = 1.25$ mm, being the light intensities at $z_0 = 0$ and at $z_6 = 1.5$ mm $= dz^G$, the light intensities at the extremes previously computed (being z_0 placed at $z = \delta$ and z_6 placed at $z = \delta\delta$, for the front glass, and z_0 placed at $z = 00$ and z_6 placed at $z = 0$, for the back glass, in Figure 1.

At the front outer glass layer, for forward collimated and diffuse light intensities, $I_c(z_6) = I_c^{\,\delta}$ and $I_d(z_6) = I_d^{\,\delta}$ using Equations (18) and (32), respectively, and $I_c(z_0) = (I_c^{\delta\delta})^*$ – computed using $I_c^{\,\delta}/\tau_c^{\,G}$ or $(1 - r_c^{\,G}) + r_c^{\,G} \cdot J_c^{\,\delta\delta}$ – and $I_d(z_0) = (I_d^{\delta\delta})^*$ – computed using $I_d^{\,\delta}/\tau_d^{\,G}$ or $r_d^{\,G} \cdot J_c^{\,\delta\delta}$ – since $I_c^{\,\delta\delta} = 1$ and $I_d^{\,\delta\delta} = 0$, and for backward collimated and diffuse light intensities, $J_c(z_0) = J_c^{\,\delta\delta}$ and $J_d(z_0) = J_d^{\,\delta\delta}$ using Equations (17) and (31), respectively, and $J_c(z_0) = (J_c^{\delta})^*$ – computed using $J_c^{\,\delta\delta}/\tau_c^{\,G}$ or $(1 - r_c^{\,GE}) \cdot J_c^{\,\delta} + r_c^{\,GE} \cdot I_c^{\,\delta}$ – and $J_d(z_0) = (J_d^{\delta})^*$ – computed using $J_d^{\,\delta\delta}/\tau_d^{\,G}$ or $(1 - r_d^{\,GE}) \cdot J_d^{\,\delta} + r_d^{\,GE} \cdot I_d^{\,\delta}$ – since $I_c^{\,\delta} \neq 1$ and $I_d^{\,\delta} \neq 0$. At the back outer glass layer, for forward collimated and diffuse light intensities, $I_c(z_6) = I_c^{\,00}$ and $I_d(z_6) = I_d^{\,00}$ using Equations (16) and (30), respectively, and $I_c(z_0) = (I_c^{\,0})^*$ – computed using $I_c^{\,00}/\tau_c^{\,G}$ or $(1 - r_c^{\,GE}) \cdot I_c^{\,0} + r_c^{\,GE} \cdot J_c^{\,0}$ – and $I_d(z_0) = (I_d^{\,0})^*$ – computed using $I_d^{\,00}/\tau_d^{\,G}$ or $(1 - r_d^{\,GE}) \cdot I_d^{\,0} + r_d^{\,GE} \cdot J_d^{\,0}$ – since $I_c^{\,0} \neq 1$ and $I_d^{\,0} \neq 0$, and for backward collimated and diffuse light intensities, $J_c(z_0) = J_c^{\,0}$ and $J_d(z_0) = J_d^{\,0}$ using Equations (19) and (33), respectively, and $J_c(z_6) = (J_c^{\,00})^*$ – computed using $J_c^{\,0}/\tau_c^{\,G}$ or $r_c^{\,G} \cdot I_c^{\,00}$ – and $J_d(z_6) = (J_d^{\,00})^*$ – computed using $J_d^{\,0}/\tau_d^{\,G}$ or $r_d^{\,G} \cdot I_d^{\,00}$ – since $J_c^{\,00} = J_d^{\,00} = 0$.

Intrinsic and extrinsic parameters were only computed for the electrolyte layer, but not for the outer glass layers, due to the low value expected for them and also because of the similitude between collimated and total T and R measurements observed with the separated glass sample, that is, in samples without scattering, $\alpha^G \approx 0$, $\varepsilon^G \approx \beta^G$, and $ACP^G \approx 1$. Hence, Equations (57) and (58) were only used for determining the total light intensities at the nine inner positions of the inner electrolyte layer, that is, from $z_1 = 2.5$ μm to $z_9 = 22.5$ μm, being the total light intensities for the five inner positions of the outer glass layers computed adding collimated and diffuse light intensities. The same gradient plots for forward and backward light intensities of the inner electrolyte layer is obtained by adding collimated and diffuse gradient plots, observed in Figures 4, 5, and 6.

Collimated light intensities decrease while crossing at the inner of the three layers of the *GEG* sample, for forward and backward light senses, as it is observed in gradient plots of Figure 4. Inner collimated and diffuse interface reflectance between glass and electrolyte layers ($r_c^{\,GE}$ and $r_d^{\,GE}$) are close to zero since a similar value for real part of refractive index was obtained for both electrolyte (n^E) and glass (n^G) layers using the procedure described in Section 3, leading to a behavior showing a

continuation in gradient plots between the different layers. The fact that $n^E \approx n^G$ causes asterisk light intensities at inner front and back interfaces (for $z = \delta$ and $z = 0$ in Figure 1) showing a similar value than light intensities without asterisk, that is, $(I_c^{\delta})^* \approx I_c^{\delta}$, $(J_c^{\delta})^* \approx J_c^{\delta}$, $(I_c^{0})^* \approx I_c^{0}$ and $(J_c^{0})^* \approx J_c^{0}$. This is not true at outer front and back interfaces (for $z = \delta\delta$ and $z = 00$ in Figure 1) since $n^G \neq n^{air}$.

The same behavior of continuation in gradients plots between the different glass and electrolyte layers is observed for the case of diffuse light intensities in Figure 5, where both diffuse forward and backward light intensities increase while crossing the layers. Hence, illuminating the *GEG* sample with collimated light from the outer front interface at $z = \delta\delta$ in Figure 1, both forward and backward collimated light intensities decrease while crossing the layers, but also both forward and backward diffuse light intensities increase while crossing the layers.

Then, for the total light intensities' gradient plots in Figure 6, the behavior is similar to collimated case, for forward light sense, and similar to diffuse case, for backward light sense, at the inner electrolyte layer. For the forward total light intensity gradient plots, in Figure 6(a), (b), and (c), total light intensity decreases when crossing the three layers of the *GEG* sample. For the backward total light intensity gradient plots, total light intensity decreases only at the outer front and back glass layers, in Figure 6(d) and (f), but not at the inner electrolyte layer, in Figure 6(e), where total backward light intensity J increases.

5. Conclusion

A thorough analysis of optical measurements for a three-substrate-layer sample, that is, *GEG* sample, consisting of two outer glass layers and an inner electrolyte layer was carried out in this paper. By fitting the collimated-collimated transmittance and reflectance equations to experimental regular transmittance and specular reflectance, the retrieved values of the optical constants of a glass sample, in a single substrate layer matrix form, were used to obtain the optical constants of the inner electrolyte layer in a three-substrate-layer matrix form. Once collimated light intensities at the interfaces were computed from glass and electrolyte optical constants using collimated interface reflectance, *CDE* of 4FM were used to obtain the same value for extinction coefficients than the retrieved using the matrix form, considering that wavelength of light at air, and not the frequency, decreases when speed of light is decreased inside glass or electrolyte substrate layers, hence using the real and imaginary parts of the complex refractive index, and not only the imaginary part, for computing the same extinction coefficients.

Then, the new method for decoupling extinction coefficients into intrinsic scattering and absorption coefficients was based on the *DDE* and the consideration of two ACPs, for forward and backward diffuse light intensities, and four FSR, for forward and backward and for collimated and diffuse light intensities. The same value in both light senses for diffuse interface reflectance, at outer and inner interfaces, were computed considering the critical angle of TIR and used for determining diffuse light intensities, required for obtaining intrinsic scattering coefficient (and hence absorption coefficient subtracting from extinction coefficients) and FSR and BSR for collimated and diffuse light intensities and forward and backward ACPs.

From intrinsic parameters, new equations based on the TDE of the 2FM were determined for extrinsic scattering and absorption coefficients and used successfully for the electrolyte inner substrate layer. Intrinsic and extrinsic retrieved parameters were used for determining collimated and diffuse, and total light intensities, respectively, required for contour diagrams of light intensities gradients. As future works, the new equations described in this work need to be tested in other samples with three-substrate-layer sandwich structure, especially for inner substrate layer with different real part of refractive index than outer substrate layers, contrary to the *GEG* sample here characterized. Finally, with a major complexity study based on the matrixial multilayer method, it would be of interest to use the new equations in multilayer samples, including more substrates and thin film layers.

The present work used the differential equations of the 4FM, for determining new equations for the intrinsic scattering and absorption coefficients. Then, from optical constants and intrinsic parameters of CDE and *DDE* of 4FM, and using the differential equations of the 2FM considered for total light components, new equations for extrinsic scattering and absorption coefficients were determined and successfully tested.

Recommendations

The reader is suggested to see the video indicated at reference [29].

Acknowledgment

The author is grateful to Laboratory for Spectroscopy of Materials of the National Institute of Chemistry of Ljubljana, for providing the *G* and *GEG* samples and the used spectrometer required for measurements, Grupo de Displays y Aplicaciones Fotónicas, Dept. Tecnología Electrónica, and the mobility grants of Universidad Carlos III de Madrid for supporting research in Slovenia.

Ethical Statement

This study does not contain any studies with human or animal subjects performed by the author.

Conflicts of Interest

The author declares that he has no conflicts of interest to this work.

Data Availability Statement

Data are available from the corresponding author upon reasonable request.

Nomenclature

Greek symbols

α	Intrinsic scattering coefficient
β	Intrinsic absorption coefficient
δ	z coordinate at front inner interface
$\delta\delta$	z coordinate at front outer interface
ϵ	Extinction coefficient obtained from optical constants
ϵ_i	Extinction coefficient obtained from forward collimated fluxes at the interfaces
ϵ_j	Extinction coefficient obtained from backward collimated fluxes at the interfaces
κ	Imaginary part of complex refractive index
λ	Wavelength

ξ Average crossing parameter (ACP)
ξ^i Average crossing parameter (ACP) for forward light flux
ξ^j Average crossing parameter (ACP) for backward light flux
σ Forward scattering ratio (FSR)
σ_c^i Forward scattering ratio (FSR) for collimated forward light flux
σ_c^j Forward scattering ratio (FSR) for collimated backward light flux
σ_d^i Forward scattering ratio (FSR) for diffuse forward light flux
σ_d^j Forward scattering ratio (FSR) for diffuse backward light flux
$(1-\sigma)$ Backward scattering ratio (BSR)
τ Fresnel transmission coefficient
τ^S Fresnel transmission coefficient for S polarization
τ^P Fresnel transmission coefficient for P polarization
τ_c^G Collimated extinction attenuation of glass substrate
τ_d^G Diffuse extinction attenuation of glass substrate
ρ Fresnel reflection coefficient
ρ^S Fresnel reflection coefficient for S polarization
ρ^P Fresnel reflection coefficient for P polarization
θ_c Critical angle for total internal reflection

English symbols

0 z coordinate at back inner interface
00 z coordinate at back outer interface
2FM Two-flux model
4FM Four-flux model
cc Collimated-collimated
cd Collimated-diffuse
CDE Collimated differential equations
dz Thickness of substrate layer
DDE Diffuse differential equations
E Electrolyte
ECD Electrochromic device
FTO Fluorine-doped tin oxide
G Glass
GEG Glass/electrolyte/glass
H Haze
i Forward light sense
I Total forward light flux
I^0 Total forward light flux at back inner interface
I^{00} Total forward light flux at back outer interface
I^δ Total forward light flux at front inner interface
$I^{\delta\delta}$ Total forward light flux at front outer interface
I_c Collimated forward light flux
I_c^0 Collimated forward light flux at back inner interface
I_c^{00} Collimated forward light flux at back outer interface
I_c^δ Collimated forward light flux at front inner interface
$I_c^{\delta\delta}$ Collimated forward light flux at front outer interface
I_d Diffuse forward light flux
I_d^0 Diffuse forward light flux at back inner interface
I_d^{00} Diffuse forward light flux at back outer interface
I_d^δ Diffuse forward light flux at front inner interface
$I_d^{\delta\delta}$ Diffuse forward light flux at front outer interface
ITO Indium-doped tin oxide
j Backward light sense
J Total backward light flux
J^δ Total backward light flux at front inner interface
$J^{\delta\delta}$ Total backward light flux at front outer interface
J^0 Total backward light flux at back inner interface
J^{00} Total backward light flux at back outer interface
J_c Collimated backward light flux
J_c^δ Collimated backward light flux at front inner interface
$J_c^{\delta\delta}$ Collimated backward light flux at front outer interface
J_c^0 Collimated backward flux light at back inner interface
J_c^{00} Collimated backward flux light at back outer interface
J_d Diffuse backward light flux
J_d^δ Diffuse backward light flux at front inner interface
$J_d^{\delta\delta}$ Diffuse backward light flux at front outer interface
J_d^0 Diffuse backward flux light at back inner interface
J_d^{00} Diffuse backward flux light at back outer interface
K Extrinsic absorption coefficient
M_{oi} Interface matrix between medium outside "o" and inside "i" mediums
N_s Substrate "s" layer matrix
n Real part of complex refractive index
n' Complex refractive index
PDLC Polymer dispersed liquid crystal
R Reflectance
r_c Collimated interface reflectance
r_d Diffuse interface reflectance
r_c^{GE} Collimated interface reflectance between glass and electrolyte
r_d^{GE} Diffuse interface reflectance between glass and electrolyte
R_{cc} Calculated specular reflectance
R_{spec} Measured specular reflectance
R_{cd} Calculated diffuse reflectance
R_{dif} Measured diffuse reflectance
R_t Calculated total reflectance
R_{tot} Measured total reflectance
T Transmittance
t_c Collimated interface transmittance
t_c^{GE} Collimated interface transmittance between glass and electrolyte
t_d^{GE} Diffuse interface transmittance between glass and electrolyte
T_{cc} Calculated regular transmittance
T_{reg} Measured regular transmittance
T_{cd} Calculated diffuse transmittance
T_{dif} Measured diffuse transmittance
T_t Calculated total transmittance
T_{tot} Measured total transmittance
TIR Total internal reflection
S Extrinsic backscattering coefficient
SPD Suspended particle device

References

[1] Bohren, C. F., & Huffman, D. R. (1983). *Absorption and scattering of light by small particles*. USA: Wiley.

[2] Mie, G. (1908). Beiträge zur Optik trüber Medien, speziell kolloidaler Metallösungen [Contributions to the optics of turbid media, particularly of colloidal metal solutions]. *Annalen der Physik*, *330*(3), 377–445. https://doi.org/10.1002/andp.19083300302

[3] Kerker, M. (1969). *The scattering of light, and other electromagnetic radiation*. USA: Academic Press.

[4] van de Hulst, H. C. (1981). *Light scattering by small particles*. USA: Dover Publications.

[5] Livesay, D. E., & Chen, K. (1974). Electromagnetic fields induced inside arbitrarily shaped biological bodies. *IEEE Transactions on Microwave Theory and Techniques*, *22*(12), 1273–1280. https://doi.org/10.1109/TMTT.1974.1128475

[6] Niklasson, G. A., Granqvist, C. G., & Hunderi, O. (1981). Effective medium models for the optical properties of inhomogeneous materials. *Applied Optics*, *20*(1), 26–30. https://doi.org/10.1364/AO.20.000026

[7] Chandrasekhar, S. (1960). *Radiative transfer*. USA: Dover Publications.

[8] Lorenzo, J. R. (2012). *Principles of diffuse light propagation: Light propagation in tissues with applications in biology and medicine*. Singapore: World Scientific. https://doi.org/10.1142/7609

[9] Ishimaru, A. (1978). *Wave propagation and scattering in random media*. USA: Academic Press.

[10] Mudgett, P. S., & Richards, L. W. (1971). Multiple scattering calculations for technology. *Applied Optics*, *10*(7), 1485–1502. https://doi.org/10.1364/AO.10.001485

[11] Niklasson, G. A. (1987). Comparison between four flux theory and multiple scattering theory. *Applied Optics*, *26*(19), 4034–4036. https://doi.org/10.1364/AO.26.004034

[12] Kubelka, P. (1948). New contributions to the optics of intensely light-scattering materials. Part I. *Journal of the Optical Society of America*, *38*(5), 448–457. https://doi.org/10.1364/JOSA.38.000448

[13] Beasley, K., Atkins, J. T., & Billmeyer Jr, F. W. (1967). Scattering and absorption of light in turbid media. In *Proceedings of the Second International Conference on Establishment Surveys: Electromagnetic Scattering,* 765.

[14] Maheu, B., Letoulouzan, J. N., & Gouesbet, G. (1984). Four-flux models to solve the scattering transfer equation in terms of Lorenz–Mie parameters. *Applied Optics*, *23*(19), 3353–3362. https://doi.org/10.1364/ao.23.003353

[15] Levinson, R., Berdahl, P., & Akbari, H. (2005). Solar spectral optical properties of pigments– Part I: Model for deriving scattering and absorption coefficients from transmittance and reflectance measurements. *Solar Energy Materials and Solar Cells*, *89*(4), 319–349. https://doi.org/10.1016/j.solmat.2004.11.012

[16] Maheu, B., & Gouesbet, G. (1986). Four-flux models to solve the scattering transfer equation: Special cases. *Applied Optics*, *25*(7), 1122–1128. https://doi.org/10.1364/ao.25.001122

[17] Saunderson, J. L. (1942). Calculation of the color of pigmented plastics. *Journal of the Optical Society of America*, *32*(12), 727–736. https://doi.org/10.1364/JOSA.32.000727

[18] Judd, D. B. (1942). Fresnel reflection of diffusely incident light. *Journal of Research of the National Bureau of Standards*, *29*(5), 329–332. https://doi.org/10.6028/jres.029.017

[19] Walsh, J. W. T. (1926). The reflection factor of a polished glass surface for diffused light. *Illumination Research Technical Paper*, *2*, 10.

[20] Kottler, F. (1960). Turbid media with plane-parallel surfaces. *Journal of the Optical Society of America*, *50*(5), 483–490. https://doi.org/10.1364/JOSA.50.000483

[21] Kortüm, G. (1969). *Reflectance spectroscopy: Principles, methods, applications*. Germany: Springer. https://doi.org/10.1007/978-3-642-88071-1

[22] Barrios, D., Alvarez, C., Miguitama, J., Gallego, D., & Niklasson, G. A. (2019). Inversion of two-flux and four-flux radiative transfer models for determining scattering and absorption coefficients for a suspended particle device. *Applied Optics*, *58*(32), 8871–8881. https://doi.org/10.1364/AO.58.008871

[23] Sagan, C., & Pollack, J. B. (1967). Anisotropic nonconservative scatttering and the clouds of Venus. *Journal of Geophysical Research*, *72*(2), 469–477. https://doi.org/10.1029/JZ072i002p00469

[24] Barrios, D., & Alvarez, C. (2023). Spectral voltage contour plots of optical constants and interface parameters of the active layer of a multilayer structure suspended particle device smart window from clear on to dark off states. *Orbital: The Electronic Journal of Chemistry*, *15*(1), 8–20. https://doi.org/10.17807/orbital.v15i1.16470

[25] Born, M., & Wolf, E. (1970). *Principles of optics: Electromagnetic theory of propagation, interference and diffraction of light*. UK: Pergamon Press.

[26] Knittl, Z. (1976). *Optics of thin films: An optical multilayer theory*. USA: Wiley.

[27] Harbecke, B. (1986). Coherent and incoherent reflection and transmission of multilayer structures. *Applied Physics B*, *39*, 165–170. https://doi.org/10.1007/BF00697414

[28] Pfrommer, P., Lomas, K. J., Seale, C., & Kupke, C. (1995). The radiation transfer through coated and tinted glazing. *Solar Energy*, *54*(5), 287–299. https://doi.org/10.1016/0038-092X(94)00132-W

[29] Barrios Puerto, D. (2023). *Forward scattering ratios, average crossing parameters and scattering and absorption coefficients new expressions using DDE of four flux model* [Streaming video]. Veoh. https://veoh.com/watch/v142259818WaRsNGn5

How to Cite: Barrios Puerto, D. (2024). Intrinsic and Extrinsic Scattering and Absorption Coefficients New Equations in Four-flux and Two-flux Models Used for Determining Light Intensity Gradients. *Journal of Optics and Photonics Research*, *1*(3), 131–144. https://doi.org/10.47852/bonviewJOPR42022261